Original article

Effect of rotational speed on structural, morphological, and optical properties of solgel spin coated Sb doped SnO₂ thin films

Darla Subramanyam^{1,2,a}, Borra Rajesh Kumar^{3,b}, Kuntalo Chandrasekhara Reddy^{1,4,c}

Corresponding author: B. Rajesh Kumar, rajindphy@gmail.com

PACS 68.55.Ln, 61.05.cp, 68.37.Hk, 68.37.Ps, 78.66.Bz, 73.61.-r

ABSTRACT Antimony doped SnO $_2$ (ATO) films were prepared on glass substrates by spin coating method at rotational speeds from 2000 to 3500 rpm. The impact of rotational speed on physical properties of Sb-doped SnO $_2$ films were reported. XRD profiles of Sb-doped SnO $_2$ films exhibits tetragonal rutile phase structure. The surface morphology shows homogeneous growth of the films with spherical structure, and an agglomeration of grains was observed at higher rotational speeds. Sb-doped SnO $_2$ films prepared at 3500 rpm show an optimum transmittance of 82 % at visible region. The optical bandgap energy of Sb-doped SnO $_2$ films were increased from 3.23 to 3.46 eV due to Burstein–Moss (B-M) effect. The electrical resistivity of Sb-doped SnO $_2$ films were increased from $2.80 \cdot 10^{-4}$ to $3.86 \cdot 10^{-4}$ Ω ·cm with an increase of rotational speed from 2000 to 3500 rpm.

KEYWORDS Sb-doped SnO₂ films, X-ray diffraction, surface morphology, optical properties, electrical properties

ACKNOWLEDGEMENTS The facilities (FESEM, AFM, and XPS) available at CeNSE, IISc, Bengaluru were utilized to perform this research work. The author also thanks to DST-FIST Program, Govt. of India for providing spectroscopic ellipsometer to GITAM.

FOR CITATION Subramanyam D., Rajesh Kumar B., Chandrasekhara Reddy K. Effect of rotational speed on structural, morphological, and optical properties of sol-gel spin coated Sb doped SnO₂ thin films. *Nanosystems: Phys. Chem. Math.*, 2025, **16** (5), 660–668.

1. Introduction

Tin oxide (SnO_2) is related to semiconductor of n-type with \sim 3.6 eV band gap, high electrical conductivity, and optical transparency [1,2]. The potential applications of SnO_2 include transparent electrodes, gas sensors, photodetectors, solar cells, etc., [3–6]. The physical properties of SnO_2 was influenced by crystallinity, defects which include oxygen vacancies, surface faults, and interstitials. The properties of SnO_2 can be varied with different conditions of synthesis methods, controlling the crystallite size, preferred crystalline growth, dopants, surface morphology, shape, and size distribution. The selection of the proper dopant in the host lattice will modify the parent system microstructure, affecting the structural, optical, and electrical properties [7–10]. Various dopants such as Cu [11], Mg [12], Sb [13] have been used to tune the properties of SnO_2 . Among these dopants, n-type doping of Sb^{3+} leads to enhancement in the conductivity, preferably substitutional cations in the Sn^{4+} site, which releases electrons leads to an increase of electron density in the conduction band (CB) [14]. Sb^{3+} state can occupy interstitial sites of SnO_2 lattice because Sb^{3+} (0.74 Å) had a larger ionic radius compared to Sn^{4+} (0.69 Å) causing a larger number of dislocations [15].

Among the several preparation methods RF/DC magnetron sputtering [16], spray pyrolysis [17,18], sol-gel [19], and SILAR [20] for doped SnO_2 . The versatile sol-gel spin coating method offers many notable benefits, such as depositing at lower temperatures, precise stoichiometry control, cost-effectiveness, deposit across the wide areas, and uniform film growth. The present work aims to study the rotational speed effect on comprehensive analysis of microstructural, morphological, optical and electrical properties of Sb-doped SnO_2 films.

¹Research and Development Centre, Bharathiar University, Coimbatore, 641046, Tamil Nadu, India

²Department of Physics, STSN Govt Degree College, Kadiri, 515591, Andhra Pradesh, India

³Department of Physics, School of Science, GITAM (Deemed to be University), Visakhapatnam, 530 045, Andhra Pradesh, India

⁴Department of Physics, Govt. Degree College, Uravakonda, 515812, Anantapur, Andhra Pradesh, India

^asubramanyamdarla@gmail.com, ^brajindphy@gmail.com, ^cchandrasekharreddyssbn@gmail.com

2. Experimental details

Sb-doped SnO₂ (ATO) films was synthesized using the chemicals SnCl₂·2H₂O, SbCl₃, and 2-methoxy ethanol as a precursor, dopant, and solvent. First, 0.2 M of SnCl₂·2H₂O and 0.05 M of SbCl₃ were mixed in 50 ml distilled water individually, and then solutions were mixed at 350 rpm for two hours at 80 °C. The precursor solution with a volume and molar ratio of [Sb]/[Sn] is 5:95 and 5 %, respectively. The monoethanolamine is used as a stabilizer and added at 5 ml/minute drop rate until a clear homogeneous solution with a pH of 9.2 is resulted. The final solution was aged for 48 hours to form a sol-gel. The final gel solutions was spin coated by using a spin coater (spinNXG-P1A, Apex Instruments Co. Pvt. Ltd, India) on glass substrates of size $2.5 \times 2.5 \text{ cm}^2$ with varying rotational speeds from 2000 to 3500 rpm. The spin-coated samples was subsequently annealed under air atmosphere at 250 °C for 10 min. Film thickness uniformity was evaluated by spectroscopic ellipsometry (J.A. Woollam, SE-Alpha, wavelength: 380 - 900 nm, 70° incidence; B-spline model, spot ~ 0.5 mm). A 9-point radial map (center, 4 mid-radius, 4 near edge) showed values ranging from 140 ± 1.8 to 235 ± 2.1 nm. X-ray diffraction patterns of ATO films were recorded using Cu K α radiation ($\lambda = 1.5406$ Å) at $2\theta =$ $10-80^{\circ}$ with a step size of 0.02° and a scan speed of 2 $^{\circ}$ /min. The surface morphology of ATO films were examined by SEM (Ultra 55, Karl Ziess) and topographic images by AFM (Model-Bruker Dimension Icon). XPS (Axis Ultra-165) is employed for elemental analysis of ATO films. The wavelength range from 200 to 2500 nm was used to measure the optical transmittance using double beam UV-VIS-NIR spectrometer (Model-Hitachi U-2900). The electrical properties of the ATO films were examined by four probe method with Keithley 2450 source meter.

3. Results and discussion

3.1. Film thickness variation with rotational speed

It is noticed that the film thickness decreased from 235 to 140 nm with the rise in rotational speed from 2000 to 3500 rpm as shown in Fig. 1. The centrifugal force on the solution increases with rotational speed increases and casts away the surplus solution to form a uniform film. The thickness of the films is inversely proportional to the rotational speed. Generally, the solutions with low viscosity will make more liquid to radial outflow and driven out from the substrate due to centrifugal force leading to thinner film.

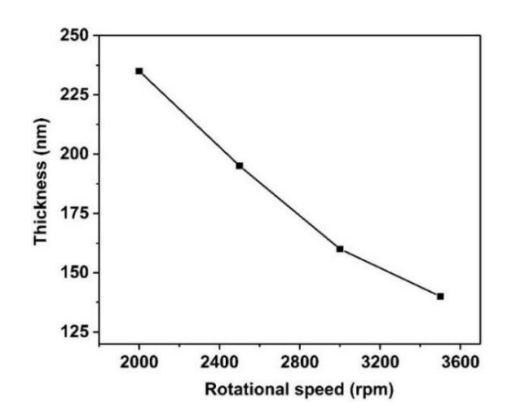


FIG. 1. Plot of film thickness with rotational speed

3.2. Structural properties

The XRD patterns of ATO films prepared at 2000, 2500, 3000, and 3500 rpm is illustrated in Fig. 2. All the peaks were matched to tetragonal cassiterite structure of SnO₂ according to the reported data in the JCPDS file no. 41-1445. No additional peaks was noticed in the spectra. The dominant spectra peaks correspond to planes (1 1 0) and (1 0 1) of Sb-doped SnO₂. It is observed from Fig. 2 that the intensities of diffraction peaks decrease with the rise in the rotational speed because the peak intensity is proportional to the film thickness [21]. Using the Debye–Scherrer relation [22], crystallite size reduced from 34 to 25 nm with the rise in spinning speed from 2000 to 3500 rpm. The decrease in crystallite size with increasing rotational speed can be attributed to the lattice stress arising from the ionic radius difference between Sn⁴⁺ (0.69 Å) and Sb³⁺ (0.74 Å) [23]. Sb³⁺ had a greater ionic radius when compared to Sn⁴⁺ it can be able to occupy at interstitial sites of the SnO₂ lattice which results in more dislocations. Sn⁴⁺ to Sb³⁺ replacement at lattice sites has the potential to enlarge the lattice due to the greater ionic radius. The lattice constants (*a* and *c*) and unit cell volume increase linearly with rotational speed in Sb-doped SnO₂ due to substitution of Sn⁴⁺ by larger Sb³⁺ ions. Similar results were observed in the previous literature ATO thin films [24, 25].

The dislocation density $\delta = [1/D^2]$, internal stress $\sigma = E \cdot \langle \varepsilon \rangle$ (SnO₂ – Young's Modulus, $E \sim 200$ GPa), and energy density strain $E_d = [0.5 \cdot E \langle \varepsilon \rangle^2]$ of ATO films were estimated [26] and reported in Table 1. The dislocation density of ATO thin films increased from $0.86 \cdot 10^{15}$ to $1.60 \cdot 10^{15}$ nm⁻² with the rise of rotational speed from 2000 to

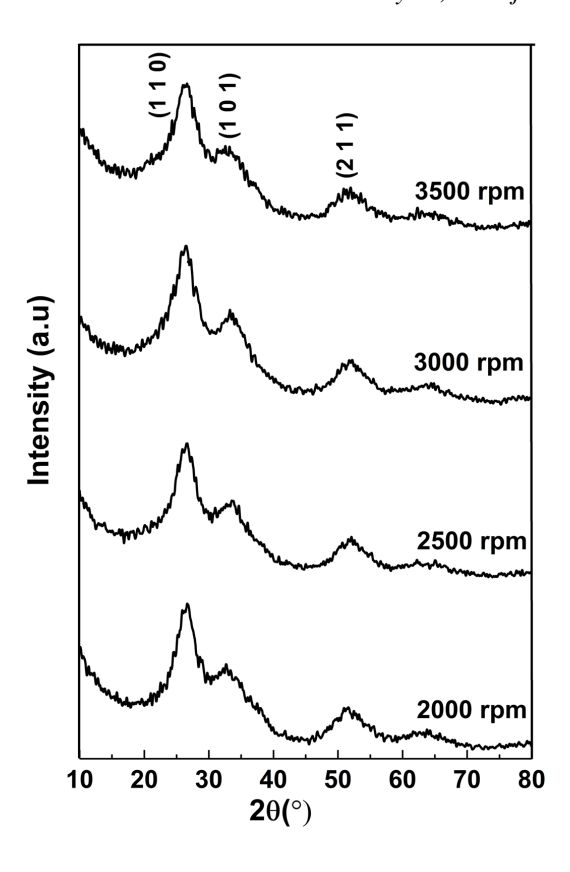


FIG. 2. XRD patterns of ATO films

3500 rpm due to grain boundary enhancement and reduced crystallite size. Other researchers also observe a similar trend in the coloration of ATO films [27, 28].

TABLE 1. Microstructural parameters of ATO films

Microstructural parameters	2000 rpm	2500 rpm	3000 rpm	3500 rpm
FWHM, β (°)	2.39	2.61	2.83	3.26
d-value (nm)	0.3356	0.3375	0.3413	0.342
Lattice constant, a (nm)	0.4746	0.4773	0.4826	0.4837
Lattice constant, c (nm)	0.3216	0.3232	0.3226	0.3281
Volume, $V = a^2 c (\mathring{A})^3$	72.46	73.65	75.14	76.77
Crystallite size, D (nm)	34	31	28	25
Microstrain, ε (line ⁻² m ⁻⁴)	1.014	1.108	1.202	1.385
Dislocation density, $\delta \cdot 10^{15} \; (\text{nm}^{-2})$	0.86	1.04	1.28	1.60
Stress, σ (GPa)	2.03	2.21	2.4	2.77
Strain energy density, $E_d \cdot 10^6 \; (\text{J} \cdot \text{m}^{-3})$	10.29	12.28	14.45	19.19

Cassiterite SnO_2 had a tetragonal rutile structure belongs to $P4_2/mnm$ (136) space groupand D_{4h}^{14} symmetry. The atomic positions u, c/a, apical and equatorial (d_1 and d_2) distances of Sn–O in the unit cell of ATO films were calculated from the following equations

$$d_1 = \sqrt{2} ua, \tag{1}$$

$$d_1 = \sqrt{2} ua, \tag{1}$$

$$d_2 = \sqrt{2\left(\frac{1}{2} - u\right)^2 \cdot a^2 + \left(\frac{c}{2}\right)^2}, \tag{2}$$

where u represents the O^{2-} ions position at $\pm(0.5+u,\ 0.5-u,\ 0.5)$ and $\pm(u,\ u,\ 0)$ [29, 30]. If c/a=2u, the Sn^{4+} cation had bond with O^{2-} anion in tetragonal configuration [31]. The basal angle (θ) was determined from the relation $\cos\theta = \left[a^2(1-4u+8u^2)-1\right]/\left[c^2+4a^2(0.5-u)^2+4a^2u^2\right]$ [32]. The variation in the d_1,d_2 values indicates more distorted octahedron symmetry, and the basal angle (θ) decreases with Sb³⁺/Sn⁴⁺ ions substitution. The obtained values of d_1,d_2 , and θ for Sb-doped SnO₂ films at various rotational speeds were reported in Table 2.

TABLE 2. Apical and equatorial $(d_1 \text{ and } d_2)$ distances, internal parameter (u), and basal angle (θ) for ATO films

Rotational speed (rpm)	Interna parameter, u	Apical distance, d_1 (Å)	Equatorial distance, $d_2(\text{\AA})$	Basal angle (θ)
2000	0.3389	2.274	1.938	24.09
2500	0.3386	2.285	1.950	23.96
3000	0.3342	2.281	1.970	23.79
3500	0.3392	2.320	1.975	23.63

3.3. Compositional analysis

XPS was used to analyse the presence of chemical elements in the ATO films. The XPS full survey spectrum in the range of electron binding energies from 0 to 1350 eV for ATO film prepared at the rotational speed of 3000 rpm is illustrated in Fig. 3(a) The peaks corresponding to Sn (4d), C (1s), Sn (3d), O (1s), Sn (3p), Sn (3s), and Sb (3d) exhibit in the XPS spectrum. The C element might be from hydrocarbons during the synthesis process. The two peaks observed at 487.1 and 495.5 eV binding energies were related to Sn $3d_{5/2}$ and Sn $3d_{3/2}$ orbitals as illustrated in Fig. 3(b). The distance between two peaks is \sim 8.4 eV, which is assigned to the Sn lattice ion in SnO₂, similar to the previous reports [33,34]. The XPS peaks at 531.4 and 542.1 eV is assigned to the trivalent states Sb $3d_{5/2}$ and Sb $3d_{3/2}$ as illustrated in Fig. 3(c) [35–37]. The XPS spectrum of O 1s is shown in Fig. 3(d). The XPS peak at 531 eV towards higher binding energy side of O 1s spectra is assigned to adsorbed oxygen species [38,39].

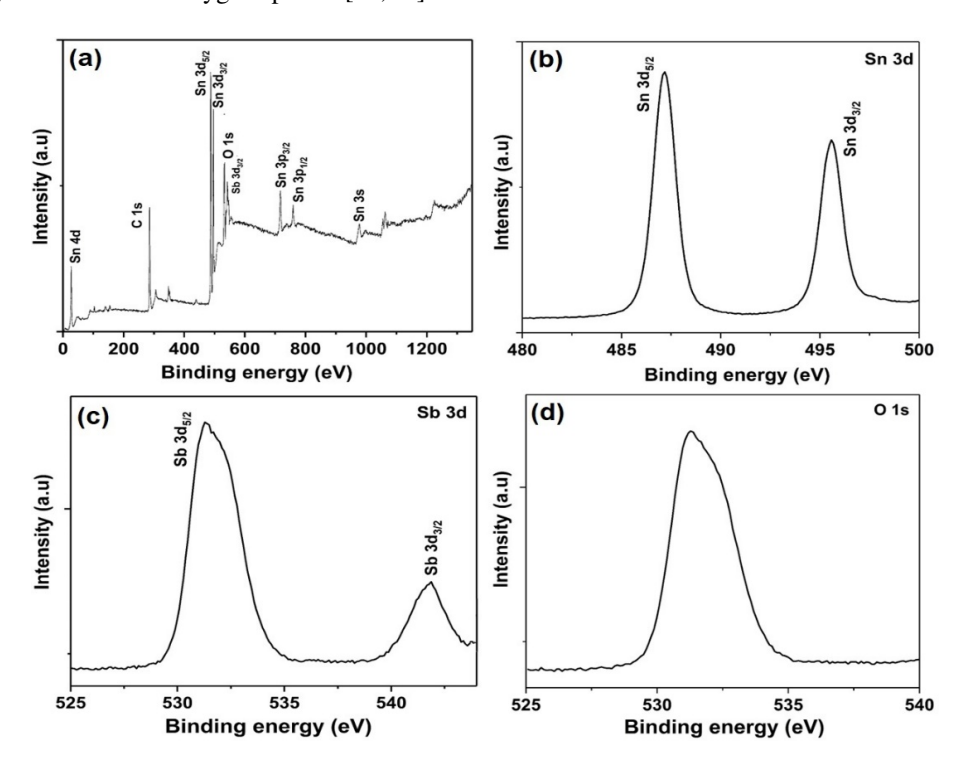


FIG. 3. XPS:(a) wide spectra, (b) Sn 3d, (c) Sb 3d, (d) O1s spectra of ATO film

3.4. Surface morphological studies

SEM images of ATO films prepared by varying rotational speeds from 2000 to 3500 is shown in Fig. 4. The surface morphology shows a dense homogeneous surface with small grains of aggregated form. The film morphology at 3000 and 3500 rpm shows an even surface of small spherical grains. The SEM images reveals that these grains are packed closely, and smaller particles consists of large surface free energy which tends to agglomerate to form enlarged grains.

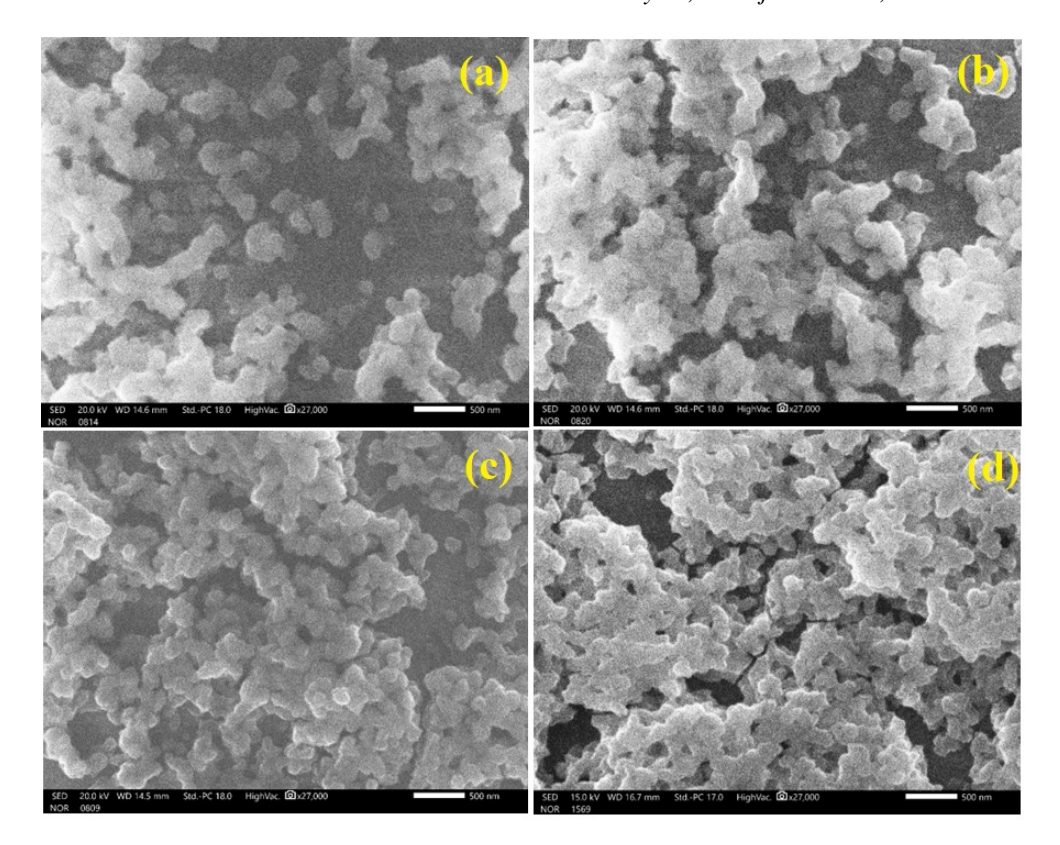


FIG. 4. SEM images of ATO films prepared at (a) 2000, (b) 2500, (c) 3000, and (d) 3500 rpm

AFM micrographs ($5 \times 5 \ \mu m^2$) displaying the surface topography of ATO films were shown in Fig. 5. The thin film samples exhibit without crack surfaces and agglomerated grains. At the higher rotational speeds many valleys and hills appeared indicating well-segregated grains. The surface roughness parameters such as R_a , R_q , R_{ku} , and R_{sk} were listed in Table 3. However, the surface skewness of ATO films is positive which indicates the presence of numerous bumps. The films prepared at higher rotational speeds had rough surfaces lacking grain growth. The surface roughness varied with increasing rotational speed due to grain size reduction, and strain arising during the grain growth. The reduced grain size degrades the crystallinity of films which confirmed with XRD analysis.

Rotational RMS roughness, Average Kurtosis, Skewness, speed (rpm) roughness, $R_a(nm)$ R_q (nm) R_{ku} R_{sk} 2000 14 11 0.63 2.33 9 2500 12 0.34 3.54 3000 11 8 0.49 2.98 3500 10 7 1.22 2.41

TABLE 3. AFM roughness parameters of ATO films

3.5. Optical properties

The optical transmittance spectra of ATO films prepared at different rotational speeds is shown in Fig. 6(a). The optical transmittance increases with increased rotational speed due to reduced film thickness from 235 to 140 nm. A smaller number of photons are being absorbed due to the decrease in thickness of the films, enhancing the film transparency. The increase in optical transmittance is due to the reduction in light scattering. The bandgap energy (E_g) of ATO films is determined from the Tauc's relation [40]:

$$(\alpha h \nu)^2 = A(h\nu - E_g)^{1/2},\tag{3}$$

where α is the absorption coefficient, $h\nu$ is the photon energy and constant A depends on the transition nature. The linear portion of Tauc's plot $(\alpha h\nu)^2$ against $h\nu$ shown in Fig. 6(b) exhibits bandgap of ATO films. It was noticed that E_g increased from 3.23 to 3.46 eV with the rise in spinning speed because of Burstein–Moss (B-M) hypothesis. The optical absorption shifts towards the higher energy which is proportional to free-electron density. The fact that the light

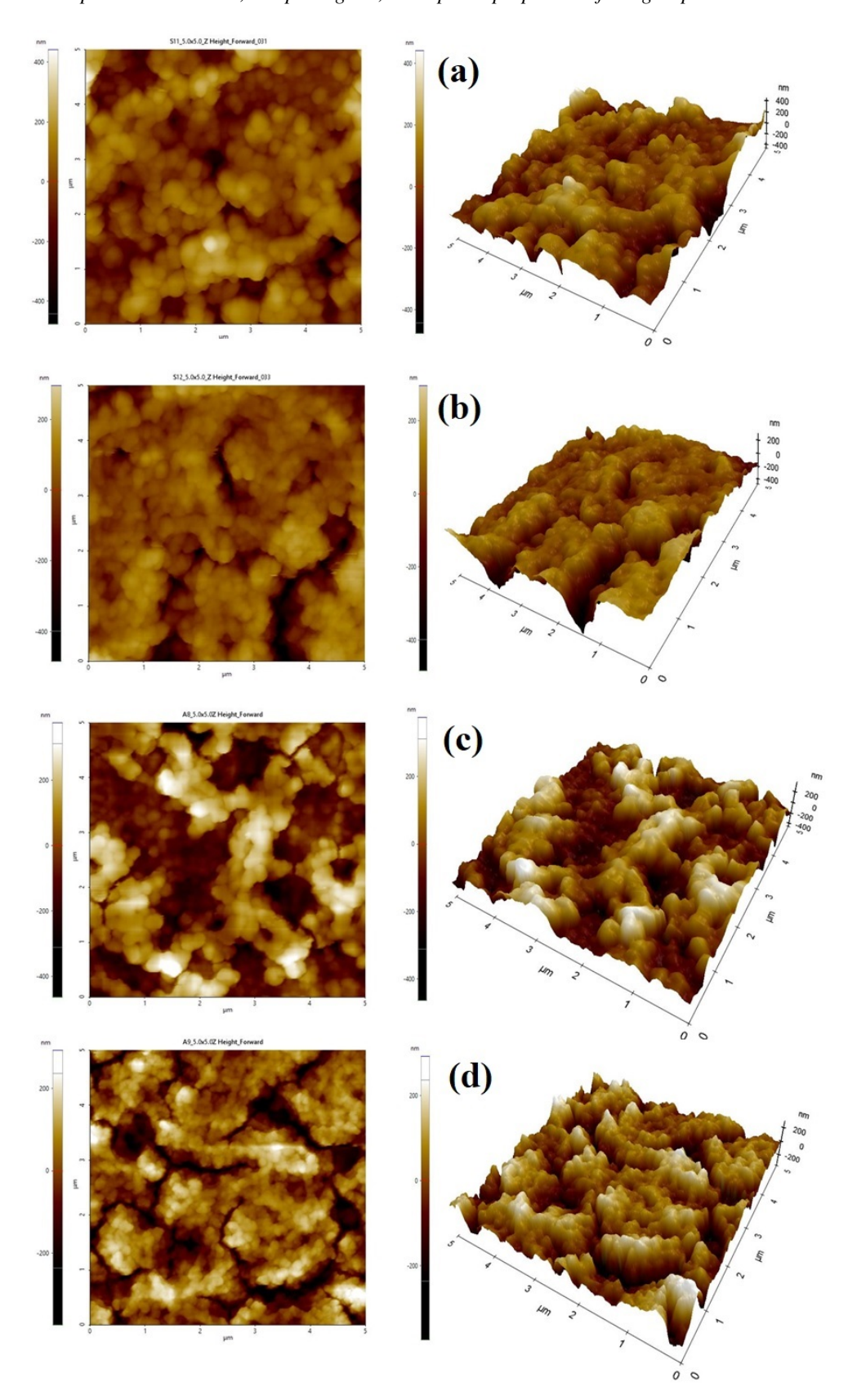


FIG. 5. AFM (2D and 3D) images of ATO films prepared at (a) 2000, (b) 2500, (c) 3000, and (d) 3500 rpm

absorption shifting towards the lower wavelengths with increasing rotational speed makes the films advantageous for its optical applications in the UV region. Similar behavior is reported by Abhijit A. Yadav et al. [41] for antimony-doped SnO₂ thin films. The optical band gap variation can be explained by B-M effect as a function of carrier concentration is given as [42]:

$$\Delta E_g^{BM} = \frac{h^2}{8m_e^*} \left(\frac{3}{\pi}\right)^{2/3} n^{2/3},\tag{4}$$

where h, m_e^* , and n represents the Planck constant, effective electron mass, and carrier concentration. The carrier concentration of ATO films were decreased from $4.44 \cdot 10^{20}$ to $3.64 \cdot 10^{20}$ cm⁻³. The decrease in carrier concentration is due to enhanced grain boundary density and comparable with AFM results [43].

The edge potentials of the conduction and valence band (E_{CB} and E_{VB}) of ATO thin films is determined from the relations [44]

$$E_{VB} = \chi - E_e + 0.5E_q, (5)$$

$$E_{CB} = E_{VB} - E_q, (6)$$

where χ (for SnO₂ \sim 6.24 eV) represents electronegativity. E_e (\sim 4.5 eV) is the free electrons energy. The E_{VB} values for ATO films prepared at 2000, 2500, 3000, and 3500 rpm are obtained as 3.355, 3.39, 3.44, and 3.47 eV, whereas the E_{CB} values are 0.125, 0.09, 0.04, and 0.01, respectively.

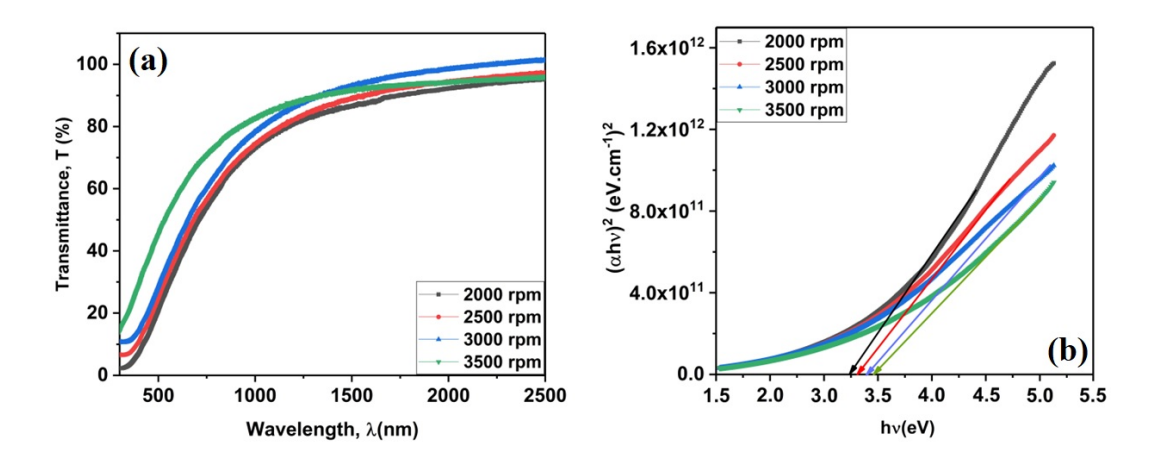


FIG. 6. (a) Optical transmittance spectra and (b) Tauc's plot of ATO films

3.6. Electrical properties

The rotational speed effect on carrier concentration (n), electrical resistivity (ρ) and mobility (μ) of ATO films is summarized in Fig. 7. The electrical resistivity of ATO films was increased from $2.80 \cdot 10^{-4}$ to $3.86 \cdot 10^{-4}$ $\Omega \cdot \text{cm}$ with an increase of rotational speed from 2000 to 3500 rpm due to reduced carrier concentration. The increase in the electrical resistivity values with an increase of rotational speed or decrease in film thickness was previously reported by Shihui Yu et al. [45]. The mobility of ATO films decreased from 50.3 to $44.5 \text{ cm}^2\text{V}^{-1}\text{s}^{-1}$ with an increase in rotational speed due to the domination by the surface scattering-limited mechanism.

4. Conclusions

Sb-doped SnO₂ thin films were successfully synthesized using the sol-gel spin coating method at different rotational speed ranges from 2000 to 3500 rpm. XRD patterns of ATO films exhibits tetragonal rutile phase with a preferred orientation along (1 0 1). The crystallite size decreased from 34 to 25 nm with an increase of rotational speed. The surface morphology of ATO films exhibits dense grains in agglomeration form. The optical transmittance of ATO films increases with an increase of rotational speed due to the decrease in the film thickness. The enhancement in the optical band gap energy from 3.23 to 3.46 eV with the rotational speed is due to the reduction in the density of defect states. The electrical resistivity of the ATO films increases from $2.80 \cdot 10^{-4}$ to $3.86 \cdot 10^{-4}$ Ω -cm with increasing rotational speed would degrade the carrier mobility of the films. The decrease in mobility of ATO films with rotational speed may be due to grain size reduction and enhancement in the grain boundary scattering. The ATO films prepared at higher rotational speed can make them suitable to be used as a transparent electrodes for the optoelectronic devices.

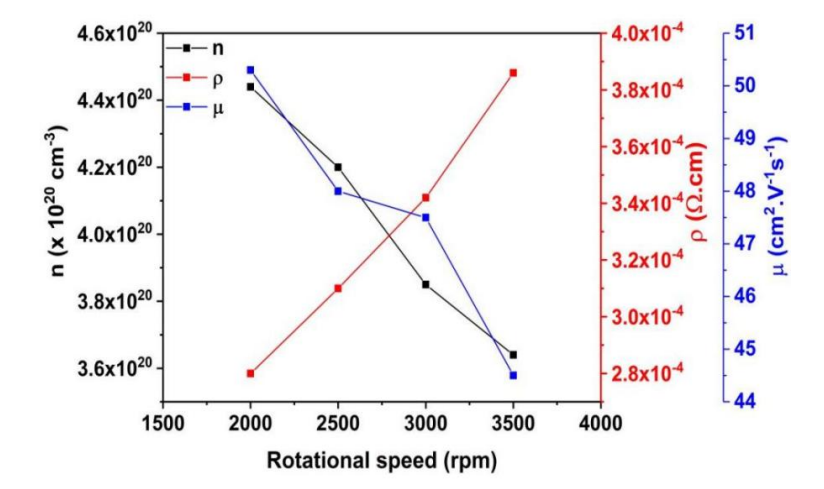


FIG. 7. Dependence of carrier concentration (n), electrical resistivity (ρ) , and mobility (μ) of ATO films

References

- [1] Manjeet Kumar, Akshay Kumar, Abhyankar A.C. Influence of Texture Coefficient on Surface Morphology and Sensing Properties of W-Doped Nanocrystalline Tin Oxide Thin Films. ACS Applied Materials & Interfaces, 2015, 7 (6), P. 3571–3580.
- [2] Towseef Ahmad, Mohd Zubair Ansari. Temperature-dependent structural and optical properties of Sb-doped SnO₂ nanoparticles and their electro-chemical analysis for supercapacitor application. New J. of Chemistry, 2024, 48, P. 8495–8509.
- [3] Asiyeh Kalateh, Ali Jalali, Mohammad Javad Kamali Ashtiani, Mohammad Mohammadimasoudi, Hajieh Bastami, Majid Mohseni. Resistive switching transparent SnO₂ thin film sensitive to light and humidity. *Scientific Reports*, 2020, **13**, P. 20036/1–11.
- [4] Rosmalini Ab Kadir, Zhenyu Li, Abu Z. Sadek, Rozina Abdul Rani, Ahmad Sabirin Zoolfakar, Matthew R. Field, Jian Zhen Ou, Adam F. Chrimes, Kourosh Kalantar-zadeh. Electrospun Granular Hollow SnO₂ Nanofibers Hydrogen Gas Sensors Operating at Low Temperatures. *The J. of Physical Chemistry C*, 2014, 118 (6), P. 3129–3139.
- [5] Xueying Kou, Chong Wang, Mengdi Ding, Changhao Feng, Xin Li, Jian Ma, Hong Zhang, Yanfeng Sun, Geyu Lu. Synthesis of Co-doped SnO₂ nanofibers and their enhanced gas-sensing properties. Sensors and Actuators B: Chemical, 2016, 236, P. 425–432.
- [6] Snaith H.J., Ducati C. SnO₂-Based Dye-Sensitized Hybrid Solar Cells Exhibiting Near Unity Absorbed Photon- to- Electron Conversion Efficiency. Nano Letters, 2010, 10 (4), P. 1259–1265.
- [7] Terrier C., Chatelon J.P., Berjoan R., Roger J.A. Sb-doped SnO₂ transparent conducting oxide from the sol-gel dip-coating technique. *Thin Solid Films*, 1995, **263** (1), P. 37–41.
- [8] Siya Haung, Hui Wu, Ming Zhou, Chunsong Zhao, Zongfu Yu, Zhichao Ruan, Wei Pan. A flexible and transparent ceramic nanobelt network for soft electronics. NPG Asia Materials, 2014, 6 (2), e86.
- [9] Lorenzi R., Brovelli S., Meinardi F., Lauria A., Chiodini N., Paleari A. Role of sol-gel networking and fluorine doping in the silica Urbach energy. *J. of Non-Crystalline Solids*, 2012, **357** (8–9), P. 1838–1841.
- [10] Arik Kar, Simanta Kundu, Amitava Patra. Surface Defect-Related Luminescence Properties of SnO₂ Nanorods and Nanoparticles. The J. of Physical Chemistry C, 2010, 115 (1), P. 118–124.
- [11] Pawan Chetri, Priyanka Basyach, Amarjyothi Choudhury. Exploring the structural and Magnetic properties of TiO₂/SnO₂ core/shell nanocomposite: An experimental and density functional study. *J. of Solid State Chemistry*, 2014, **220**, P. 124–131.
- [12] Mazumder N., Bharati A., Saha S., Sen D., Chattopadhyay K.K. Effect of Mg doping on the electrical properties of SnO₂ nanoparticles. *Current Applied Physics*, 2012, **12** (3), P. 975–982.
- [13] Qi Wei, Peng Song, Zhuoqi Li, Zhongxi Yang, Qi Wang. Hierarchical peony-like Sb-doped SnO₂ nanostructures: Synthesis, characterization and HCHO sensing properties. *Materials Letters*, 2017, **191**, P. 173–177.
- [14] Towseef Ahmad, Mohd Zubair Ansari. Structural and optical characteristics of Sb doped SnO₂ nanoparticles and their boosted photocatalytic activity under visible light irradiation. Ceramics Int., 2023, 49 (22), P. 35740–35756.
- [15] Martinez-Gazoni R.F., Allen M.W., Reeves R.J. Conductivity and transparency limits of Sb-doped SnO₂ grown by molecular beam epitaxy. *Physical Review B*, 2018, **98** (15), 155308.
- [16] Bo Xu, Xiao-Guang Ren, Guang-Rui Gu, Lei-Lei Lan, Bao-Jia Wu. Structural and optical properties of Zn-doped SnO₂ films prepared by DC and RF magnetron co-sputtering. *Superlattices and Microstructures*, 2016, **89**, P. 34–42.
- [17] Indira Gandhi T., Ramesh Babu R., Ramamurthi K. Structural, morphological, electrical and optical studies of Cr doped SnO₂ thin films deposited by the spray pyrolysis technique. *Materials Science in Semiconductor Processing*, 2013, **16** (2), P. 472–479.
- [18] Ibrahim N.B., Abdi M.H., Abdullah M.H., Baqiah H. Structural and optical characterization of undoped and chromium doped tin oxide prepared by sol-gel method. *Applied Surface Science*, 2013, **271**, P. 260–264.
- [19] Mejda Ajili, Michel Castagné, Najoua, Kamoun Turki. Spray solution flow rate effect on growth, optoelectronic characteristics and photoluminescence of SnO₂:F thin films for photovoltaic applications. *Optik*, 2015, **126** (7–8), P. 708–714.
- [20] Irmak Karaduman Er., Memet Ali Yıldırım, Hasan Örkçü H., Aytunç Ateş, Selim Acar. Structural morphological and gas sensing properties of Zn_{1-x}Sn_xO thin films by SILAR method. Applied Physics A, 2021, 127 (4), P. 230/1-14.
- [21] Karthik T.V.K., Hernandez A.G., de la Olvera M.L., Maldonado A., Gómez Pozos H. Effect of Au and Ag contacts on the CO sensitivity of SnO₂ thick films. *J. of Materials Science: Materials in Electronics*, 2020, **31**, P. 7481–7489.
- [22] Ali Yıldırıma M., Sümeyra Tuna Yıldırımb, Emine Fedakar Sakara, Aytunç Atesc. Synthesis, characterization and dielectric properties of SnO₂ thin films. Spectrochimica Acta Part A: Molecular and Biomolecular Spectroscopy, 2014, 133, P. 60–65.

- [23] Shimin Liu, Jindong Liu, Bin Wen, Weiwei Jiang, Chaoqian Liu, Wanyu Ding, Hualin Wang, Nan Wang, Zhihua Zhang, Weiping Chai. Structural, morphological, electrical and optical properties of SnO₂ nanoparticles: influence of Sb doping. *J. of Materials Science: Materials in Electronics*, 2016. 27. P. 6932–6938.
- [24] Ahmad A. Ahmad, Migdadi A.B., Qais M. Al-Bataineh. Structural, optical, and electrical properties of strontium doped tin oxide films for high photoconductivity. *Thin Solid Films*, 2024, **796**, 140312.
- [25] Sibel Gürakar, Tülay Serin. High quality optoelectronic properties of Sb-doped SnO₂ by spray pyrolysis with less solution. *Materials Research Express*, 2019, **6** (8), 086423.
- [26] Subramanyam D., Rajesh Kumar B., Chandrasekhar Reddy K. Micro-Structural, Surface Morphological, and Optical Properties of Sol–Gel Spin Coated Sb-Doped SnO₂ Thin Films. *Physics of the Solid State*, 2025, **67**, P. 17–26.
- [27] Elangovan E., Shivashankar S.A., Ramamurthi K. Studies on Structural and electrical properties of sprayed SnO₂: Sb films. J. of Crystal Growth, 2005. 276. P. 215–221.
- [28] Masahiko Kojima, Hisao Kato, Mitsuru Gatto. Blackening of tin oxide thin films heavily doped with antimony. *Philosophical Magazine Part B*, 1993, **68**, P. 215–222.
- [29] Hamad B.A. First-principle calculations of structural and electronic properties of rutile-phase dioxides (MO₂), M = Ti, V, Ru, Ir and Sn. *The European Physical J. B*, 2009, **70**, P. 163–169.
- [30] Aashish Kumar, Naveen Kumar, Mansi Chitkara, Gulshan Dhillon. Physicochemical investigations of structurally enriched Sm³⁺ substituted SnO₂ nanocrystals. J. of Materials Science: Materials in Electronics, 2022, 33, P. 5283–5296.
- [31] Soumen Das, Jayaraman V. SnO₂: A comprehensive review on structures and gas sensors. Progress in Materials Science, 2014, 66, P. 112-255.
- [32] Aragon F.H., Coaquira J.A.H., Villegas-Lelovsky L., da Silva S.W., Cesar D.F., Nagamine L.C.C.M., Cohen R., Menendez-Proupin E., Morais P.C. Evolution of the doping regimes in the Al-doped SnO₂ nanoparticles prepared by a polymer precursor method. *J. of Physics: Condensed Matter*, 2015, 27 (9), 095301.
- [33] Liwei Wang, Jintao Li, Yinghui Wang, Kefu Yu, Xingying Tang, Yuanyuan Zhang, Shaopeng Wang, Chaoshuai Wei. Construction of 1D SnO₂-coated ZnO nanowire heterojunction for their improved n-butylamine sensing performances. *Scientific Reports*, 2016, **6** (1), 35079.
- [34] Meihua Li, Chao Mou, Yunfan Zhang, Xiao Li, Huichao Zhu, Guangfen Wei. Zn-doped SnO₂ nanoparticles for ethanol vapor sensor: a combined experimental and first principles study. *J. of Materials Science: Materials in Electronics*, 2023, **34** (12), 1059.
- [35] Yang Q., Tang K., Wang C., Qian Y., Yu W., Zhou G., Li F. Antimony sulfide tetragonal prismatic tubular crystals. *J. of Materials Chemistry*, 2011, 11 (2), P. 257–259.
- [36] Kang Xiao, Qi-Zhi Xu, Kai-Hang Ye, Zhao-Qing Liu, Lu-Miao Fu, Nan Li, Yi-Bo Chen, Yu-Zi Su. Facile Hydrothermal Synthesis of Sb₂S₃ Nanorods and their magnetic and Electrochemical properties. ECS Solid State Letters, 2013, 2 (6), P. 51–54.
- [37] Yanfen Niu, Libing Duan, Xiaoru Zhao, Cong Han, Jiale Guo, Wangchang Geng. Effect of Sb doping on structural and photoelectric properties of SnO₂ thin films. *J. of Materials Science: Materials in Electronics*, 2020, **31** (48), 3289.
- [38] Wu J.M. A room temperature ethanol sensor made from p-type Sb-doped SnO₂ nanowires. Nanotechnology, 2010, 21 (23), 235501.
- [39] Babar A.R., Shinde S.S., Moholkar A.V., Bhosale C.H., Kim J H., Rajpure K.Y. Structural and optoelectronic properties of antimony incorporated tin oxide thin films. *J. of Alloys and compounds*, 2010, **505** (2), P. 416–422.
- [40] Ali Yıldırım M., Aytunç Ates. Influence of films thickness and structure on the photo-response of ZnO films. *Optics Communications*, 2010, **283** (7), P. 1370–1377.
- [41] Abhijit A. Yadav. Influence of film thickness on structural, optical, and electrical properties of spray deposited antimony doped SnO₂ thin films. *Thin Solid Films*. 2015. **591**. P. 18–24.
- [42] Mariem Chaari, Adel Matoussi. Effect of Sn₂O₃ doping on structural, optical and dielectric properties of ZnO ceramics. *Materials Science and Engineering B*, 2013, **178**, P. 1130–1139.
- [43] Junji Sawahata, Tasuku Kawasaki. Structural and electrical properties of Sb-doped SnO₂ thin films prepared by metal organic decomposition. *Thin Solid Films*, 2019, **685**, P. 210–215.
- [44] Wang J., Lu C., Liu X., Wang Y., Zhu Z., Meng D. Synthesis of tin oxide (SnO & SnO₂) micro/nanostructures with novel distribution characteristic and superior photocatalytic performance. *Materials & Design*, 2017, **115**, P. 103–111.
- [45] Shihui Yu, Linghong Ding, Chuang Xue, Li Chen Li, Zhang W.F. Transparent conducting Sb-doped SnO₂ thin films grown by pulsed laser deposition. *J. of Non-Crystalline Solids*, 2012, **358** (23), P. 3137–3140.

Submitted 10 April 2025; revised 5 September 2025; accepted 6 October 2025

Information about the authors:

Darla Subramanyam – Research and Development Centre, Bharathiar University, Coimbatore, 641046, Tamil Nadu, India; Department of Physics, STSN Govt Degree College, Kadiri, 515591, Andhra Pradesh, India; ORCID 0009-0004-5805-6266; subramanyamdarla@gmail.com

Borra Rajesh Kumar – Department of Physics, School of Science, GITAM (Deemed to be University), Visakhapatnam, 530 045, Andhra Pradesh, India; ORCID 0000-0002-3015-6001; rajindphy@gmail.com;

Kuntalo Chandrasekhara Reddy – Research and Development Centre, Bharathiar University, Coimbatore, 641046, Tamil Nadu, India; Department of Physics, Govt. Degree College, Uravakonda, 515812, Anantapur, Andhra Pradesh, India; ORCID 0000-0002-2445-8054; chandrasekharreddyssbn@gmail.com;

Conflict of interest: the authors declare no conflict of interest.